ELSEVIER

#### Contents lists available at ScienceDirect

#### **Biomaterials**

journal homepage: www.elsevier.com/locate/biomaterials



# Novel H<sub>2</sub>S-Releasing hydrogel for wound repair via *in situ* polarization of M2 macrophages



Jiang Wu<sup>a,b,1</sup>, Anqi Chen<sup>a,1</sup>, Yajiao Zhou<sup>a</sup>, Sen Zheng<sup>a</sup>, Yao Yang<sup>b</sup>, Ying An<sup>a</sup>, Ke Xu<sup>a,b</sup>, Huacheng He<sup>b,\*</sup>, Jianming Kang<sup>d</sup>, Jittima Amie Luckanagul<sup>e</sup>, Ming Xian<sup>d,\*\*</sup>, Jian Xiao<sup>a,\*\*\*</sup>, Qian Wang<sup>c,\*\*\*</sup>

- a School of Pharmaceutical Sciences, Key Laboratory of Biotechnology and Pharmaceutical Engineering, Wenzhou Medical University, Wenzhou, Zhejiang, 325035, China
- <sup>b</sup> College of Chemistry and Materials Engineering, Wenzhou University, Wenzhou, Zhejiang, 325027, PR China
- <sup>c</sup> Department of Chemistry and Biochemistry, University of South Carolina, Columbia, SC, 29208, United States
- <sup>d</sup> Department of Chemistry, Washington State University, Pullman, WA, 99164, United States
- <sup>e</sup> Research Unit for Plant-produced Pharmaceuticals and the Department of Pharmaceutics and Industrial Pharmacy, Faculty of Pharmaceutical Sciences, Chulalongkorn University, 254 Phayathai Rd., Wangmai, Pathumwan, Bangkok, 10330, Thailand

#### ARTICLE INFO

# Keywords: Hydrogen sulfide HA hydrogels Wound healing pH responsive M2 macrophage Controlled release

#### ABSTRACT

Hydrogen sulfide ( $H_2S$ ), as a gaseous messenger, exhibits potential therapeutic effects in biological and clinical applications. Herein, an *in situ* forming biomimetic hyaluronic acid (HA) hydrogel was used as a matrix to dope a pH-controllable  $H_2S$  donor, JK1, to form a novel HA-JK1 hybrid system. This HA-JK1 hydrogel was designed as an ideal delivery scaffold for JK1 with pH-dependent prolonged  $H_2S$  releasing profile. *In vitro* study suggested that JK1 could induce the polarization of M2 phenotype indicating a higher pro-healing efficiency of macrophages. The *in vivo* studies on dermal wounds showed that the HA-JK1 hybrid hydrogel significantly accelerated the wound regeneration process through enhanced re-epithelialization, collagen deposition, angiogenesis and cell proliferation. Furthermore, the *in vivo* results also demonstrated a higher level of M2 polarization in HA-JK1 treated group with reduced inflammation and improved wound remodeling effects, which was consistent with the *in vitro* results. These observations could be considered as a key to the efficient wound treatment. Therefore, we suggest that HA-JK1 can be used as a novel wound dressing material toward cutaneous wound model *in vivo*. This system should significantly enhance wound regeneration through the release of  $H_2S$  that induces the expression of M2 macrophage phenotype.

#### 1. Introduction

Skin plays pivotal role in protecting against environmental damage and microbial invasion [1]. Cutaneous injuries, especially chronic wounds, burns and infectious wounds, require immense financial burden to healthcare systems due to the lack of satisfactory management [2]. Various drugs including growth factor [3–5], stem cell [6,7], siRNA [8,9], DNA [10,11] and gasotransmitter [12–14] have been pursued to accelerate the wound efficacy. In addition, different delivery systems including polymers [6,15], nanofibers [16,17], hydrogels [18–21], micelle [22,23], and nanoparticles [24,25] have been

investigated for the effective delivery of wound healing drugs. Among all these delivery systems, hydrogels have attracted increasing interests due to their 3D porous network and highly hydration capability that facilitate the exchange of oxygen, nutrients and provide a moist environment for epidermal migration [26,27]. In particular, *in situ* forming hydrogels are the most promising hydrogel systems for wound healing applications because the pre-gel can be injected to fill any irregular defect before gelation [28].

Restoration of skin after injury involves cellular interactions between multiple cell types following sequential regenerative phases [29]. The acute wound healing process experiences temporally

 $<sup>\</sup>ensuremath{^{\circ}}$  Corresponding author.

<sup>\*\*</sup> Corresponding author.

<sup>\*\*\*</sup> Corresponding author.

<sup>\*\*\*\*</sup> Corresponding author.

E-mail addresses: hehc@wzu.edu.cn (H. He), mxian@wsu.edu (M. Xian), xfxj2000@126.com (J. Xiao), wang263@mailbox.sc.edu (Q. Wang).

<sup>&</sup>lt;sup>1</sup> These authors contributed equally to this work.

overlapping phases including inflammation, proliferation and remodeling [30]. Excessive delayed inflammation is one of the main pathogenic mechanisms of unhealed wounds [31]. It is known that macrophage is one of the most essential inflammatory cells in wound healing process. They can be activated into two different phenotypes: M1, inflammatory phenotype in early stage, and M2, anti-inflammatory phenotype in the mid-stage [32]. Appropriate drugs which can tune the macrophage from M1 to M2 would potentially promote wound regeneration to coordinate the skin repair process. In addition to the reduction of initial inflammation, this activation of subsequent regeneration phase such as proliferation and remolding also plaved vital roles in the wound healing process [33-35]. Hydrogen sulfide (H<sub>2</sub>S), the newly recognized gasotransmitter, has shown great therapeutic potential in biomedical studies due to its anti-inflammation effect [36-40]. As a small molecular signaling motif, H<sub>2</sub>S could immediately exert its therapeutic effects by travelling through cell membranes. One of the mechanisms responsible for its therapeutic effects is the promotion of macrophage phenotype transition towards M2 macrophages [37,41,42]. However, commonly used H<sub>2</sub>S donors showed uncontrollable release of H<sub>2</sub>S [43,44]. Thus, different kinds of H<sub>2</sub>S donors, which can release H<sub>2</sub>S in a biological environment-responsive manner, have been developed for different applications [45,46]. Recently, an innovative H<sub>2</sub>S donor referred to as JKs has been developed by our group (M. Xian) which shows a pH dependent H<sub>2</sub>S releasing behavior. This pH-responsive releasing property is particularly applicable for acute wound healing treatment since the pH change upon wound microenvironment [47] can potentially switch the H<sub>2</sub>S release. Briefly, in the early inflammation stage, acidic pH could be detected at wound site which inhibits bacterial growth, decreases proteolytic activity, and promotes fibroblast growth. However, local pH gradually shifts to the basic range during the subsequent proliferation process. Thus, in the initial inflammatory phase, the low pH can trigger the release of H<sub>2</sub>S releasing from the JK-donors. For example, we recently fabricated an novel electrospinning biodegradable PCL nanofibers loading JK1 to investigate the effects of H2S exerting on the wound healing process in vivo. It was revealed that controlled H2S release from JK1 in wound helped the re-epithelialization, granulation formation and collagen deposition during the wound healing process [14]. However, we found that the PCL nanofibers matrix itself is too hydrophobic and exhibited poor oxygen permeability impeded the wound regeneration efficiency. More importantly, the underlying wound healing mechanism of H<sub>2</sub>S from JK1 is still unclear.

In this work, a hyaluronic acid (HA) based hydrogel was used to encapsulate JK1. The gelation time of the HA-hydrogel can be controlled which greatly facilitates the application at irregular shaped wounds. Additionally, as a major constituent of extracellular matrix (ECM) of HA, the biocompatible JK1-HA wound dressings [48–50] provide high oxygen and nutrients permeability and humidity [51] for *in vivo* wound healing. We also performed *in vitro* and *in vivo* experiments to investigate JK1 on polarization of macrophages. Our results proved that JK1 could significantly up-regulate the M2 polarization of macrophages, which likely contributes to an improved wound healing process.

#### 2. Materials and methods

#### 2.1. Materials and reagents

Dulbecco's modified Eagle's medium (DMEM) was purchased from Sigma-Aldrich (St. Louis, MO, USA). Fetal bovine serum (FBS) was obtained from Hyclone (UT, USA). Phosphate buffer saline (PBS), penicillin and streptomycin were purchased from Gibco BRL, Invitrogen Corp., (Carlsbad, CA, USA). Murine interleukin-4 (IL-4) was obtained from PeproTech (Jiangsu, China). Bovine serum albumin (BSA), DAPI, hematoxylin, eosin, RIPA lysis buffer and PMSF proteinase inhibitor were purchased from Beyotime® Biotechnology (Shanghai, China).

Bicinchoninic acid (BCA) reagent was obtained from Thermo (Rockford, IL, USA). Polyvinylidene fluoride (PVDF) membrane and fat free milk were purchased from Bio-Rad (Hercules, CA, USA). Triton X-100 and Masson's trichrome staining kit were obtained from Solarbio Science & Technology Co., Ltd. (Beijing, China). Primary antibodies to CD206, TNF-\alpha, cytokeratin, CD68, CD31 and Ki67, and secondary antibodies for fluorescence staining were purchased from Abcam (Cambridge, UK). Goat anti-rabbit (H + L) HRP secondary antibody was purchased from Bioworld Technology (St. Louis, MO, USA). TRIzol reagent was purchased from Invitrogen (Carlsbad, CA, USA). PrimeScript™ RT reagent kit was purchased from Takara Bio Inc. (Shiga. Japan). Methacrylic anhydride was purchased from Macklin Biochemical Co., Ltd. (Shanghai, China), Hyaluronic acid (HA) was purchased from Liuzhou Shengqiang Biotech Co., Ltd (Liuzhou, Guangxi, China). Dithiothreitol (DTT) was purchased from Aladdin (Shanghai, China). Biopsy punches were obtained from Acuderm® inc., (Ft Lauderdale, FL, USA). 3 M Tegaderm Films were obtained from 3 M Health Care (Germany).

#### 2.2. Cell experiments

#### 2.2.1. Cell lines and cell cultures

Mouse monocyte macrophages of cell line Raw 264.7 were purchased from American Type Culture collection and cultivated in DMEM (pH 7.4) containing 10% fetal bovine serum FBS, 100 unit/mL penicillin and 100  $\mu$ g/mL streptomycin in a controlled incubator at 37 °C with an atmosphere of 5% CO<sub>2</sub>.

#### 2.2.2. JK1treatment on Raw 264.7 macrophages

2.2.2.1. Cell morphologies. Raw 264.7 macrophages were seeded at  $5.0 \times 10^4$  cells per well in 6-well plates and cultured for 48 h at 37 °C followed by the replacement of medium by fresh medium (2 mL/well) with the addition of JK1 solution at various concentration of 25, 50, 100, 20, 500  $\mu$ M, respectively. Images of cell morphologies were captured by a Nikon microscope (Nikon, Tokyo, Japan).

2.2.2.2. Cell immunofluorescence. Raw 264.7 macrophages were treated with JK1 solution as mention above for 48 h. The medium was then carefully removed and washed three times with PBS. Cells were fixed with 4% paraformaldehyde for 30 min at 4 °C, and incubated in 5% BSA containing 0.1% Triton X-100 for 40 min at 37 °C. After that, cells were incubated with a rabbit polyclonal antibody to CD206 (1:1000, ab64693, Abcam) diluted in PBS containing 1% BSA overnight at 4 °C. Cells were then thoroughly washed with PBS and incubated with a donkey anti-rabbit IgG Alexa Fluor® 488-conjugated secondary antibody (1:1000, ab150073, Abcam) diluted in PBS at 37 °C for 1 h in the dark. Finally, cells were stained with DAPI to visualize the nuclei. Fluorescence images were captured using a Nikon confocal laser microscope (Nikon, A1 PLUS, Tokyo, Japan).

2.2.2.3. Western blot. Total cell lysates of Raw 264.7 macrophages were obtained using RIPA lysis buffer containing 1% PMSF on ice for 20 min. After 12,000 g centrifugation at 4 °C, the supernatant was collected to quantify the protein concentration using BCA reagents. Protein samples were separated through a 12% Bis-Tris polyacrylamide gel and transferred onto a PVDF membrane. Then PVDF membranes were blocked with 5% fat free milk in TBST [10 mM Tris-HCl (pH 7.6), 100 mM NaCl and 0.1% Tween 20] for 2 h at room temperature and incubated with a rabbit polyclonal antibody to CD 206 (1:1000, ab64693, Abcam) in 5% milk in TBST overnight at 4 °C. The membranes were washed with TBST 3 times and incubated with a goat anti-rabbit horseradish peroxidase-conjugated secondary antibody for 2 h at room temperature. The proteins on the PVDF membranes were visualized by ChemiDicTM XRS + Imaging System (Bio-Rad), and the signal intensities of the immunoreactive bands were quantified using Multi Gauge Software of Science Lab 2006 (FUJIFILM

Corporation, Tokyo, Japan). The relative intensities of the bands were analyzed with Quantity One (version 4.5.2; Bio-Rad). Quantities of band intensities were normalized using GAPDH.

2.2.2.4. Reverse transcription-polymerase chain reaction (RT-PCR). RAW264.7 cells after treatment were washed with cold PBS and incubated with TRIzol reagent for 10 min on ice. Total cell lysates were collected, added with chloroform and left for 3min. After centrifugation, isopropyl alcohol was added to the supernatant for another 10 min. After centrifugation, the sediment was washed with ethyl alcohol for twice to finally get pure RNA. Reverse transcription of total RNA was conducted using PrimeScript™ RT reagent kit following the manufacturer's instructions. The amplification reaction was performed using a qPCR thermal cycler (Bio-Rad, MyCycler, CA, USA). Primer sequences are listed below. Primers were generated for IL-6 (forward: 5'-CCAATGCTCTCCTAACAGAT-3', reverse: 5'-TGTCCA CAAACTGATATGCT-3') and iNOS (forward: 5'-CGCTTGGG TCTTGTTCACT-3', reverse: 5'-TCTTTCAGGTCACTTTGGTA-3') Realtime quantitative polymerase chain reaction (PCR) was then performed on a real-time fluorescent quantitative PCR System (QuantStudio 3, Thermo, USA).

2.2.2.5. Flow cytometric analysis. After treatment of JK1 (100 μM) and IL-4 (40 nM) on Raw 264.7 macrophages for 48 h,  $1\times 10^6$  cells of the control group, the JK1 group and the IL-4 group were incubated with 1 μg Alexa Fluor® 647 anti-mouse CD206 antibody (141711, Biolegend) diluted in staining buffer for 30 min on ice in dark. Afterwards, cells were washed twice by staining buffer to remove excess antibodies, followed by the resuspension with 500 μL staining buffer. Stained cells were analyzed using a FACS Calibur flow cytometer (BD Biosciences) and the CellQuest software (Pharminogen). Data were analyzed using FlowJo software.

#### 2.3. Hydrogel preparation and examination in vitro

#### 2.3.1. H<sub>2</sub>S releasing hyaluronic acid hydrogel formation

The HA with molecular weight 47 kDa was firstly functionalized via the reaction with methacrylic anhydride following the literature [28,52,53]. HA hydrogel was formed by crosslinking methacrylated hyaluronic acid (MeHA). The polymer was completely dissolved in PBS (pH 7.4) to the concentration of 40 g/L and the pH of the solution was adjusted to 8. To 500  $\mu$ L of this solution, DTT (10  $\mu$ L, 0.5 M) was added as a cross-linker, followed by the addition of the H<sub>2</sub>S donor, JK1 storage solution (40  $\mu$ L, 200 mM). After sufficient dissolution, the reaction mixture was injected into the mold and then kept at the room temperature. After standing for 30 min through the cross-linking reaction between the double bond within the HA, the final HA-JK1 hydrogel was obtained and transferred to a 6-well culture plate at room temperature for further analysis and application.

#### 2.3.2. Mechanical property measurements of hydrogels

The rheological characterization of the HA based hydrogels was performed using a DHR-3 rheometer (TA instrument) with parallel plate geometry (12 mm diameter) under temperature-controlled peltier. The rheometer was set to the oscillatory mode at frequency of  $10 \, \text{rad/s}$  and a controlled strain of 2% in order to monitor the continual crosslinking process with structural transformation through the transition of the mechanical property. The gelling time was determined by the intersection of G' and G'' modulus curves.

#### 2.3.3. Characterization and analysis of hydrogels

SEM images of the freeze-dried hydrogels were obtained using a scanning electron microscopy (SEM, VEGA3 TESCAN). In short, hyaluronic acid hydrogel samples were dried by liquid  $N_2$ , followed by being gold-sputtered under vacuum using a Desk II gold sputter coater (Denton Vacuum, Morristown, NJ) for 60 s. At least three random areas

were chosen to observe the morphology of the hydrogels. The elemental analysis via energy dispersive X-ray (EDX) spectra were examined under the same condition using the scanning electron microscopy. Moreover, Fourier transform infrared spectrometry (FTIR) of HA-JK1 hydrogels, HA hydrogels alone and JK1 was conducted using a Spectrum 100 (FT-IR) Spectrometer.

#### 2.3.4. Hydrogen sulfide release at different pH

The release kinetics of hydrogen sulfide from the donor JK1 and JK1 loaded HA hydrogels were examined at predetermined time points. 100 mg JK1 loaded hydrogels and 100 mg JK1 were immersed in 10 mL PBS under different pH (pH 7.4 and pH 6.0). At each time point, 0.1 mL aliquots was withdrawn and added to the mixture of zinc acetate (50  $\mu$ L, 1% w/v in H $_2$ O) and NaOH (6.25  $\mu$ L, 1.5 M) in 1.5 mL centrifuge tubes. After centrifugation at 20,500 rcf for 1 h, the supernatant was removed. FeCl $_3$  (100  $\mu$ L, 30 mM in 1.2 M HCl), and N,N-dimethyl-phenylenediamine sulfate (100  $\mu$ L, 20 mM in 7.2 M HCl) was added to centrifuge tubes. With addition of water (1 mL), solutions were transferred to 96-well plate and the optical density was measured at 670 nm after 20 min.

#### 2.4. Wound healing in vivo

#### 2.4.1. Animal model for dermal wound healing

Male C57BL/6 mice (8-12 weeks) were used in this study which were obtained from the Laboratory Animals Center of Wenzhou Medical University. All procedures were conducted according to international ethical guidelines and the National Institutes of Health Guide concerning the Care and Use of Laboratory Animals. Mice were anesthetized with 4% chloral hydrate and the dorsal skin was shaved and then sterilized with 70% ethanol. Two silicone rings with an internal diameter of 8 mm and thickness of 0.5 mm were stitched on the dorsal skin of each mouse, where two full-thickness wounds were made with a 6-mm biopsy punch per mice. Mice were randomly divided into three groups: group I was treated with 0.9% saline, group II with HA hydrogels, and group III with JK1 loaded HA hydrogels. HA Hydrogels with a diameter of 7 mm were applied directly to each wound and then the wound was covered with a sheet of 3 M Tegaderm Film and fixed with medical bandages. Photographs of the wounds were taken on day 0, 7, 10, 14, 17, 20 after surgery and analyzed using Image-Pro plus. Mice were sacrificed after anesthesia on day 7 and 20, and wound tissues were excised and fixed in 4% paraformaldehyde at 4°C for 24 h followed by paraffin embedding and sectioning at a thickness of 5 µm using a microtome (LEICA RM2235, Germany).

#### 2.4.2. Hematoxylin and eosin staining

Sections were deparaffinized in xylene for 30 min and rehydrated in descending ethanol series (100%, 95% and 80%), and distilled water for 5 min respectively. Samples were submerged in hematoxylin for 5 min, followed by 3 min in PBS to reduce the background staining. Sections were then stained with eosin for 2 min, followed by 5 min in distilled water, 5 min in 80%, 90% and 100% ethanol respectively for dehydration, and 15 min in xylene. Slides were mounted with neutral resin and coverslipped. The stained sections were observed and images were captured using a Nikon microscope (Nikon, Tokyo, Japan).

#### 2.4.3. Masson's trichrome staining

Sections were deparaffinized and rehydrated as mentioned above and then stained using Masson's trichrome staining kit following the manufacturer's suggested protocols. Briefly, the cell nuclei were stained with A1:A2 (1:1) for 5 min, and then sections were thoroughly rinsed with water and submerged in acid alcohol for differentiation for 3 s. Ponceau acid fuchsin solution was used to stain fibrous tissue for 5 min, followed by 1 min in 2% acetic acid solution, 30 s in phosphomolybdic acid solution for differentiation, and 20 s in aniline blue, after which sections were dehydrated, mounted and cover-slipped as mentioned

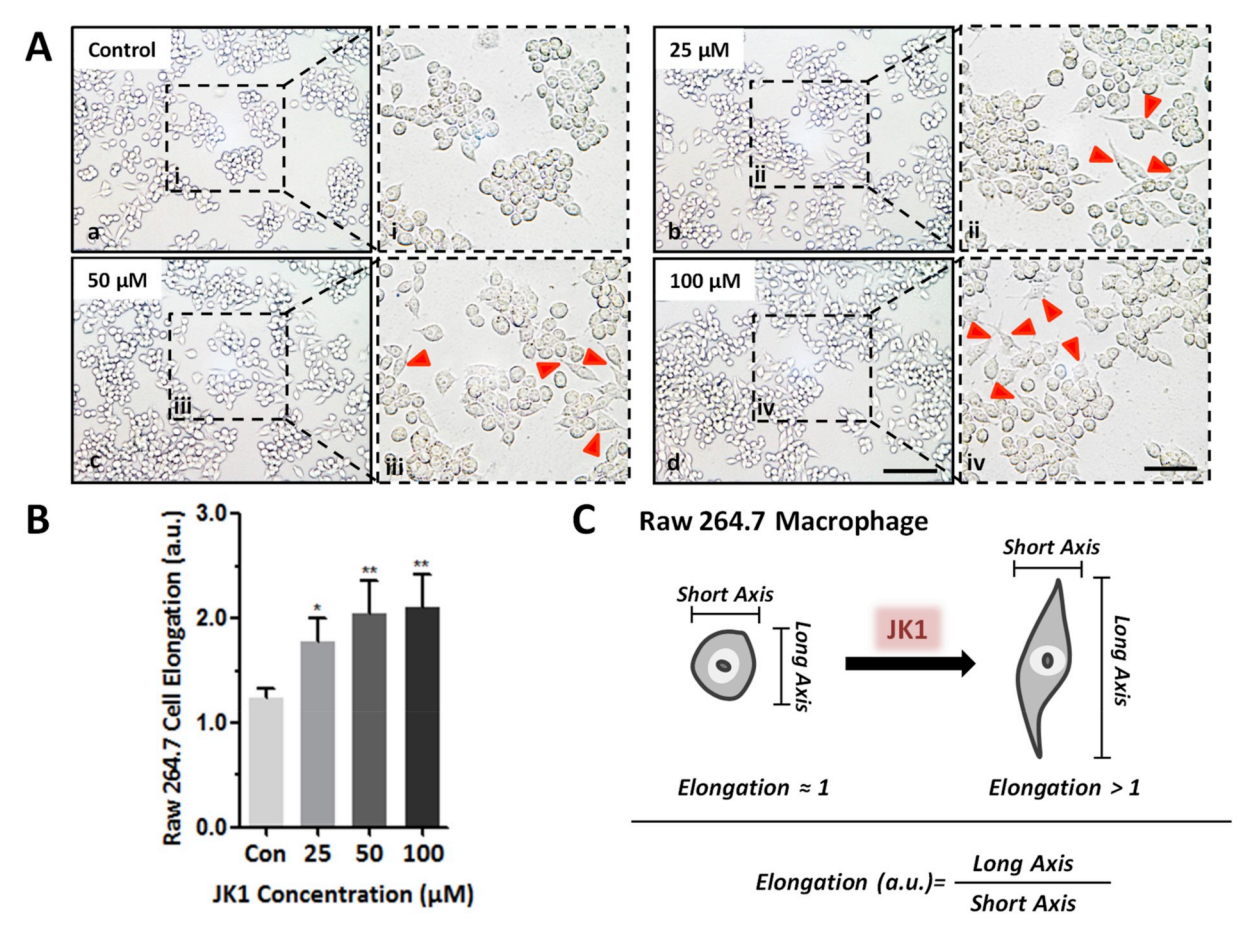


Fig. 1. JK1 treatment induced morphological change of macrophages *in vitro*. (A) Cell morphological change of Raw 264.7 macrophages after 24 h's exposure to JK1 at various concentrations observed by optical microscope. Red arrowheads indicated elongated macrophages. Scale bar:  $100 \,\mu\text{m}$  (a–d);  $50 \,\mu\text{m}$  (i-iv). (B) Statistical data of the cell elongation change of Raw 264.7 macrophages showed in (A), n > 5. (C) The schematic of the cell morphological change affected by JK1 treatment (Cell elongation was defined as a ratio of long axis length to short axis length). Statistical differences were performed using one-way analysis of variance (ANOVA). \*\*P < 0.01, \*P < 0.05, compared to control group. (For interpretation of the references to colour in this figure legend, the reader is referred to the Web version of this article.)

above. The stained sections were observed and images were captured using a Nikon microscope (Nikon, Tokyo, Japan). Three stained sections of each group were measured by the integrated optical density (IOD) of blue stained collagen fibers per unit area (mm<sup>2</sup>) using Image-Pro Plus 6.0 software.

#### 2.4.4. Immunohistochemical staining

After deparaffinization and rehydration, the endogenous peroxidase of the sections was inactivated with 3% hydrogen peroxide at room temperature for 15 min and the nonspecific binding sites were blocked with 5% BSA at 37 °C for 30 min. Sections were incubated with a rabbit polyclonal antibody to cytokeratin (1:300, ab9377, Abcam) diluted in PBS containing 1% BSA at 4 °C overnight and washed with PBS, followed by incubation with a goat anti-rabbit (H + L) HRP secondary antibody (1:1000, BS13278, Bioworld) diluted in PBS at 37 °C for 60 min. Sections were then counterstained with hematoxylin and mounted with neutral resin. Images were captured by a Nikon microscope (Nikon, Tokyo, Japan) and analyzed using an Image-Pro Plus software (Nikon, Tokyo, Japan).

#### 2.4.5. Immunofluorescence staining

After deparaffinization and rehydration, followed by the blocking of the nonspecific binding sites as described above, sections were incubated with a rabbit polyclonal antibody to CD31 (1:200, ab28364, Abcam), a rabbit polyclonal antibody to Ki67 (1:100, ab15580, Abcam), a rabbit polyclonal antibody to CD 206 (1:1000, ab64693, Abcam), a

mouse polyclonal antibody to CD68 (1:200, ab955, Abcam) and a rabbit polyclonal antibody to TNF-α (1:100, ab6671, Abcam) diluted in PBS containing 1% BSA at 4°C overnight respectively. After being washed with PBS, sections were then incubated with a donkey anti-rabbit IgG Alexa Fluor® 488-conjugated secondary antibody (1:1000, ab150073, Abcam), a donkey anti-mouse IgG Alexa Fluor® 647-conjugated secondary antibody (1:1000, ab150111, Abcam), and a donkey anti-rabbit IgG Alexa Fluor® 647-conjugated secondary antibody (1:1000, ab150075, Abcam) diluted in PBS at 37 °C for 60 min in the dark, corresponding to the first antibodies. After being counterstained with DAPI and mounted with antifade mounting medium, fluorescent images of the sections were taken using a Nikon confocal laser microscope (Nikon, A1 PLUS, Tokyo, Japan). Each fluorescent microscope images was evaluated for the positive expression using Image-Pro Plus 6.0 software. For Ki67 positive cell level analysis, more than five immunofluorescence-stained sections were measured for the count of red immunofluorescence-stained samples per unit area (mm<sup>2</sup>) using Image-Pro Plus 6.0 software.

#### 3. Statistical analysis

All data were expressed as mean  $\pm$  standard deviations (SD). Statistical differences were performed using one-way analysis of variance (ANOVA) followed by Tukey's test with GraphPad Prism 5 software (GraphPad Software Inc., La Jolla, CA, USA). For all tests, \*p value < 0.05, \*\*p value < 0.01, \*\*\*p value < 0.001.

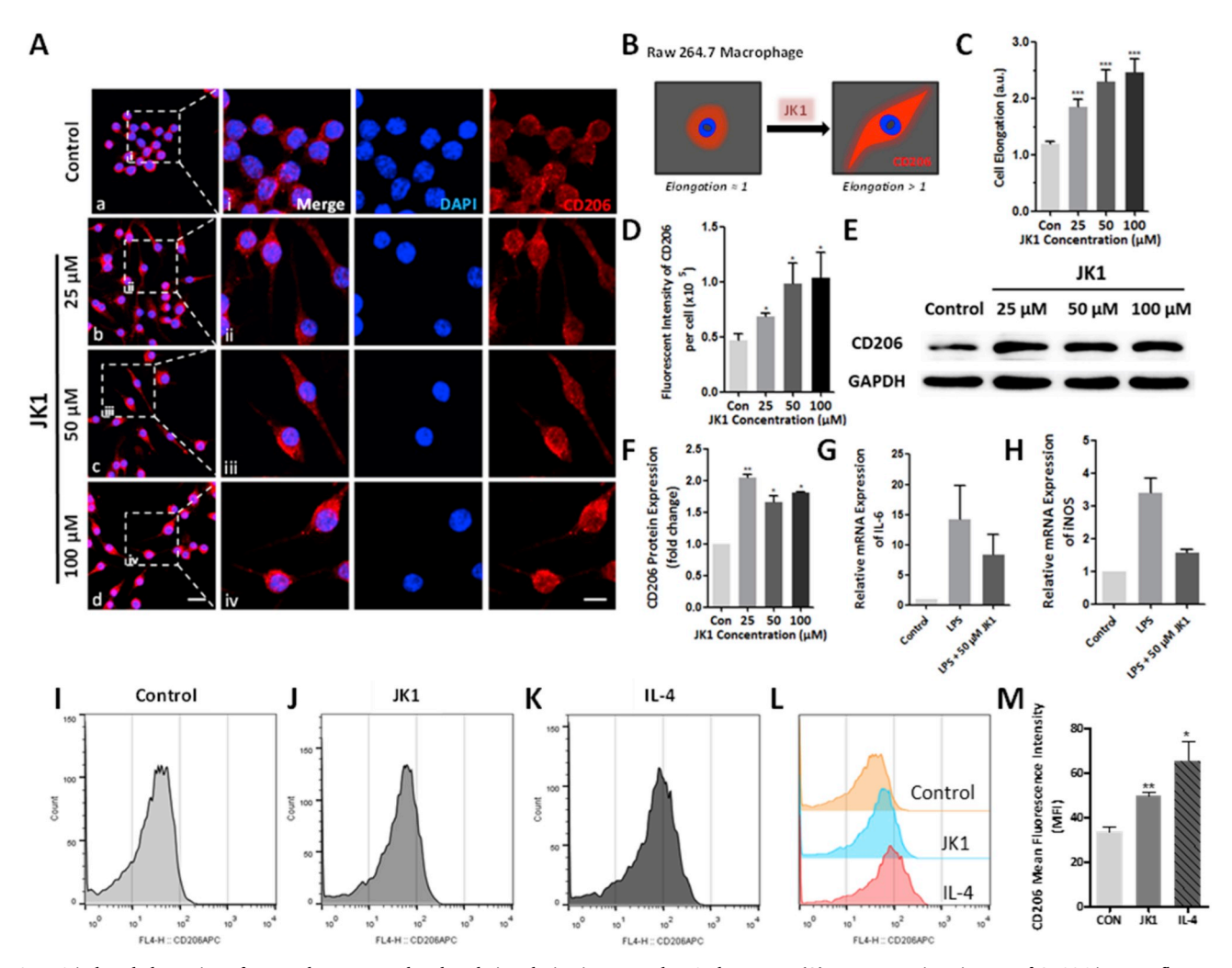


**Fig. 2.** JK1-induced elongation of macrophages was related to their polarization towards M2 phenotype. (**A**) Representative pictures of CD206 immunofluorescence staining of Raw 264.7 after 48 h's JK1 treatment at the concentration of 0, 25, 50 and 100 μM. Figure a–d share the scale bar of 10 μm, magnified pictures of 5 μm. (**B**) The schematic of the cell morphological change and the elevated expression of CD206 affected by JK1 treatment. (**C**) Statistical data of the cell elongation change of Raw 264.7 macrophages shown in (**A**), n > 5. (**D**) Statistical data of CD206 fluorescence intensity of the control group and JK1 treated groups, n > 5. (**E**) Protein expression level of CD206 conducted by western blotting in the macrophages treated with JK1 at various concentrations for 48 h, compared to control group. (**F**) Quantification of western blotting bands in (**E**), n = 3. (**G and H**) Relative mRNA expression of IL-6 and iNOS in the macrophages treated with LPS (500 ng/mL, 12 h) with or without the pretreatment of JK1 (50 μM, 24 h), n = 3. (**I–L**) Histograms of CD206 expression after treatment of JK1 or IL-4 for 48 h by flow cytometric analysis. (**M**) Mean Fluorescence Intensity (MFI) of CD206 in the three groups, n = 3. Statistical differences were performed using one-way analysis of variance (ANOVA). \*\*\*P < 0.001, \*\*P < 0.01, \*P < 0.05, compared to control group.

#### 4. Results and discussion

#### 4.1. JK1 pursued the polarization of macrophages to M2 phenotype in vitro

Macrophage cells, as a prominent inflammatory cell type in wounds, are known to have many functions toward wound. And their different phenotypes have been described closely related to the wound remolding, scarring and fibrosis [54,55]. On one hand, deficiency in M2 polarization is relative to some pathological process including chronic non-healing wounds such as diabetic ulcers, since M2 macrophages serve inflammation resolving and regeneration promoting functions [56]. On the other hand, it has been demonstrated that anti-inflammation of H2S is through its actions by driving macrophage differentiation towards M2 (anti-inflammatory) phenotype [41,42]. Therefore, we firstly tested the biological effect of H<sub>2</sub>S donor JK1 on its polarization of macrophages to M2 phenotype in vitro on Raw 264.7 macrophages. Macrophages were incubated with JK1 at different concentrations (0, 25, 50, and 100 µM) for 24 h and then morphologies were observed under an optical microscope. Fig. 1A-a showed that macrophages cultured in medium without the addition of JK1 appeared

morphologically round and clustered. With the increase of JK1 concentration, more macrophages with elongated shape (indicated with red arrowheads in magnified photos ii-iv) and loosely compact cells could be observed (Fig. 1A-b, c and d). Thereafter, Fig. 1B showed the schematic figure describing JK1 treated group with altered macrophages' morphology from a round shape to an elongated shape. The control group exhibited elongation of 1.2  $\pm$  0.1, while the 100  $\mu$ M JK1 group showed that of 2.1  $\pm$  0.3, which was 1.7 times higher than the control. This enhanced elongation of macrophages is considered to be closely related to the M2 macrophage phenotypes with anti-inflammatory property [57,58]. Previous study demonstrated that macrophages underwent morphological alteration under the stimulus of different molecular signals [59]. When stimulated with LPS and IFN- $\gamma$ , which are recognized M1 polarization inducers, macrophages displayed a round shape. However, M2 polarization inducers such as IL-4 had elongating effects on macrophages. The morphological alteration of macrophages had connection with their functional polarization states that elongated macrophages tended to polarize into M2 macrophages and inhibited M1 polarization [60,61]. The schematic diagram in Fig. 1C concluded the effect of JK1 on the cellular shape of

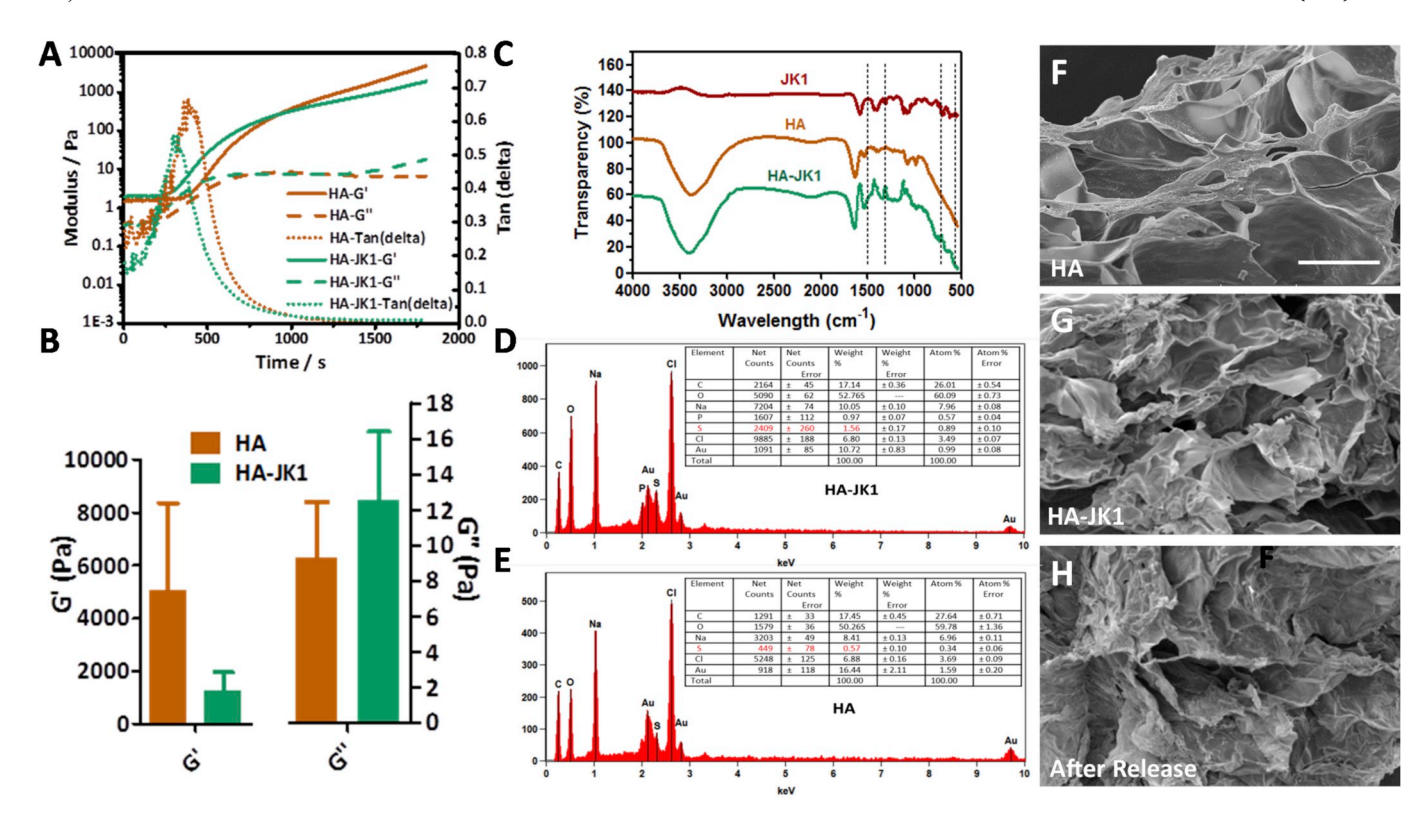


Fig. 3. Physical and chemical characteristics of HA-JK1 hydrogel. (A and B) Storage modulus (G') and loss modulus (G'') of hyaluronic acid (HA) hydrogel alone and JK1 loaded HA hydrogel, n = 3. (C) FTIR spectra of JK1, HA hydrogel and HA-JK1 hydrogel. (D and E) EDX spectra examination of HA hydrogel (D) and HA-JK1 hydrogel (E). (F–H) Representative SEM images of HA hydrogel alone (F), HA-JK1 hydrogel (G) and HA-JK1 hydrogel after releasing JK1 (after 48 h's incubation in solution) (H). Scale bar represents 50 μm.

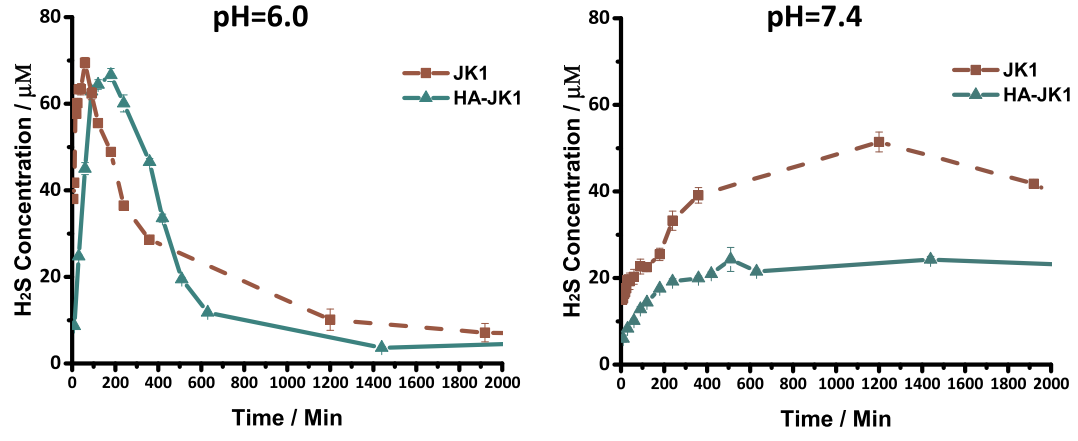


Fig. 4.  $H_2S$  releasing profile of JK1 and HA-JK1 hydrogel under pH 6.0 (A) and 7.4 (B), n > 3.

macrophages.

Further investigations related to the state of macrophages by performing immunofluorescence staining of CD206, a surface marker of M2 macrophages, were carried out to confirm the M2 phenotype polarization of JK1. As shown in Fig. 2A, after the exposure to JK1 at concentrations of 25, 50, and  $100\,\mu\text{M}$  for 48 h, Raw 264.7 macrophages exhibited an obvious change of cell shape, stretched out to the sides appearing pseudopod-like structures, in contrast to the round shape of the control group. Statistically, JK1 treated macrophages showed significantly elevated degree of cell elongation than untreated cells (Fig. 2B). More importantly, elongated macrophages treated with JK1 had significantly higher average CD206 fluorescence intensity (Fig. 2D), indicating the polarization state of macrophage is related to M2 phenotype [62]. Western blotting was conducted to further demonstrate the effects of JK1 on macrophage polarization. After 48 h

JK1 treatment at various concentrations, the expression levels of CD206 were elevated (Fig. 2E and F). These findings suggest that JK1 can induce the macrophage polarization to M2 anti-inflammatory type with elongated cell morphology and increased expression of M2 phenotype maker *in vitro*. The H<sub>2</sub>S-releasing JK1 could further serve as a prohealing M2 macrophage inducer to modulate the polarization of the macrophages associated with wound healing process. To further confirm our hypothesis, we treated macrophages with LPS (lipopoly-saccharide), a potent inducer of M1 polarization [63], and found that the pretreatment of JK1 for 24 h partly counteracted the effect of LPS, indicated by the lower levels of IL-6 and iNOS compared to the LPS positive control group (Fig. 2G–H). We performed flow cytometry to further verify the M2 polarization after JK1 treatment. CD206 were here chosen as M2 macrophage marker. Interleukin-4 (IL-4) was previously reported as a potent inducer of CD206 + M2 macrophages

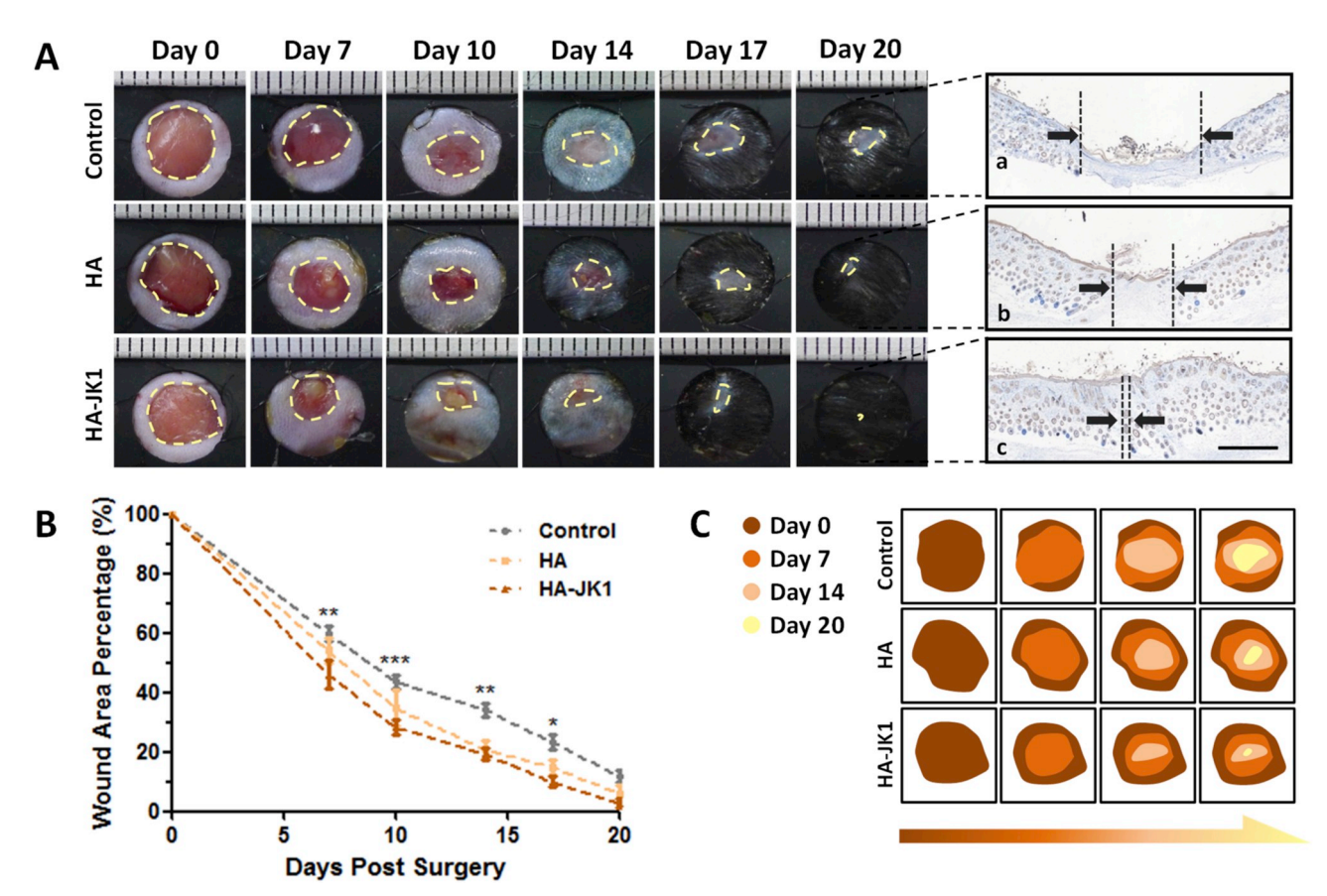


Fig. 5. HA-JK1 hydrogel accelerated *in vivo* dermal wound healing. (A) Representative images of wounds of the control group, HA hydrogel group and HA-JK1 hydrogel group at each pre-determined time point post wounding. Macroscopic wound areas were circled in yellow dotted lines. The unit of the rulers over the pictures represents 1 mm. Figures a-c represented immunohistochemical staining of keratin of wound tissue on day 20 post wounding. (B) Statistical data of wound area percentages of the three groups at different time point,  $n \ge 5$ . (C) Schematic diagram of the healing process of the three groups on day 0, 7, 14 and 20 post wounding. Statistical differences were performed using one-way analysis of variance (ANOVA). \*\*\*P < 0.001, \*\*P < 0.01, \*P < 0.05, compared to control group. (For interpretation of the references to colour in this figure legend, the reader is referred to the Web version of this article.)

[64,65], thus we used IL-4 as positive control to verify the effect of JK1. Representative histograms showed CD206 expressing levels in the control group (Fig. 2I), JK1 group (Fig. 2J) and positive control IL-4 group (Fig. 2K). Compared with the untreated macrophages, JK1 treatment increased the fluorescence intensity of CD206 antigen (Figure 2L), same with the positive control of IL-4. Specifically, it was observed that in Figure 2M, compared with the control macrophages with mean fluorescence intensity (MFI) of CD206 (33.3  $\pm$  2.3), JK1 significantly enhanced the MFI to 49.5  $\pm$  1.6, whereas MFI of CD206 in the IL-4 group was  $65.3 \pm 9.0$ . To further verify the M2 polarization effect of JK1, all the studies were repeated with primary mouse peritoneal macrophages (MPMs) isolated from C57BL/6 mice shown in Fig. S1, which confirmed that JK1 effectively drives M2 macrophage polarization in macrophages in vitro. Additionally, flow cytometric analysis on bone marrow derived macrophages (BMDMs) also showed the function of JK1 on M2 polarization (Fig. S2). All the results of Raw 264.7 together with those of primary MPMs and BMDMs strongly proved that our JK1 exerted the function of promoting macrophage polarization towards M2 phenotype.

#### 4.2. Characteristics of HA-JK1 hydrogel

JK1 was loaded into HA hydrogel before applied to wound *in vivo*. The rheological studies showed that two key parameters of the physical properties of hydrogels, the storage modulus (G') and loss modulus (G''), which represent the energy stored and dissipated per unit strain, respectively, were not statistically different for HA hydrogel and HA-JK1 (Fig. 3A–B). The intersection of G' and G'' curves represented the

transformation at gelation point (time) of two hydrogels that were also comparable, which were around  $366.3 \pm 22.2 \, \mathrm{s}$  for HA and  $336.2 \pm 17.6 \, \mathrm{s}$  for HA-JK1. By comparing the data between HA-JK1 hydrogel and HA hydrogel alone, it is found that loading JK1 into HA hydrogels did not affect much rheological property of HA hydrogels.

In order to prove the successful loading of H<sub>2</sub>S donor JK1 within the HA hydrogel, the Fourier Transform Infrared Spectrometry (FTIR) spectrum was conducted (Fig. 3C). Compared to HA hydrogel, distinctive additional absorption peaks of HA-JK1 hydrogel located at wavelengths of 1540 and 690 cm<sup>-1</sup> resulting from amidic N-H bending and aromatic C-H bending, similar to JK1 only, were appeared, suggesting JK1 was already loaded into the HA hydrogel. The energy dispersive X-ray (EDX) was also employed to further confirm the existence of JK1 by elemental analysis (Fig. 3D-E). HA-JK1 hydrogel exhibited a higher sulfur peak compared with HA hydrogel alone. Additionally, there was a characteristic phosphorus peak in HA-JK1 hydrogel which didn't exist in the single HA hydrogel. These additional elemental peaks owing to JK1, further determined the successful loading of JK1 within HA hydrogel. With these evidences, H<sub>2</sub>S donor JK1 had achieved its inclusion in HA hydrogel and the new  $\mathrm{H}_2\mathrm{S}$  releasing hydrogel system named HA-JK1 was successfully obtained.

The porous structures of freeze-dried hydrogels were observed by SEM (Fig. 3F–H), representing the morphologies of the single HA hydrogel, HA-JK1 hydrogel and HA-JK1 hydrogel after releasing JK1, respectively. No obvious morphological difference could be seen between HA hydrogel and HA-JK1 hydrogel, indicating that the encapsulation of JK1 had no impact on the inner porous structure of HA hydrogel, while the porous-structure became looser and slightly swollen

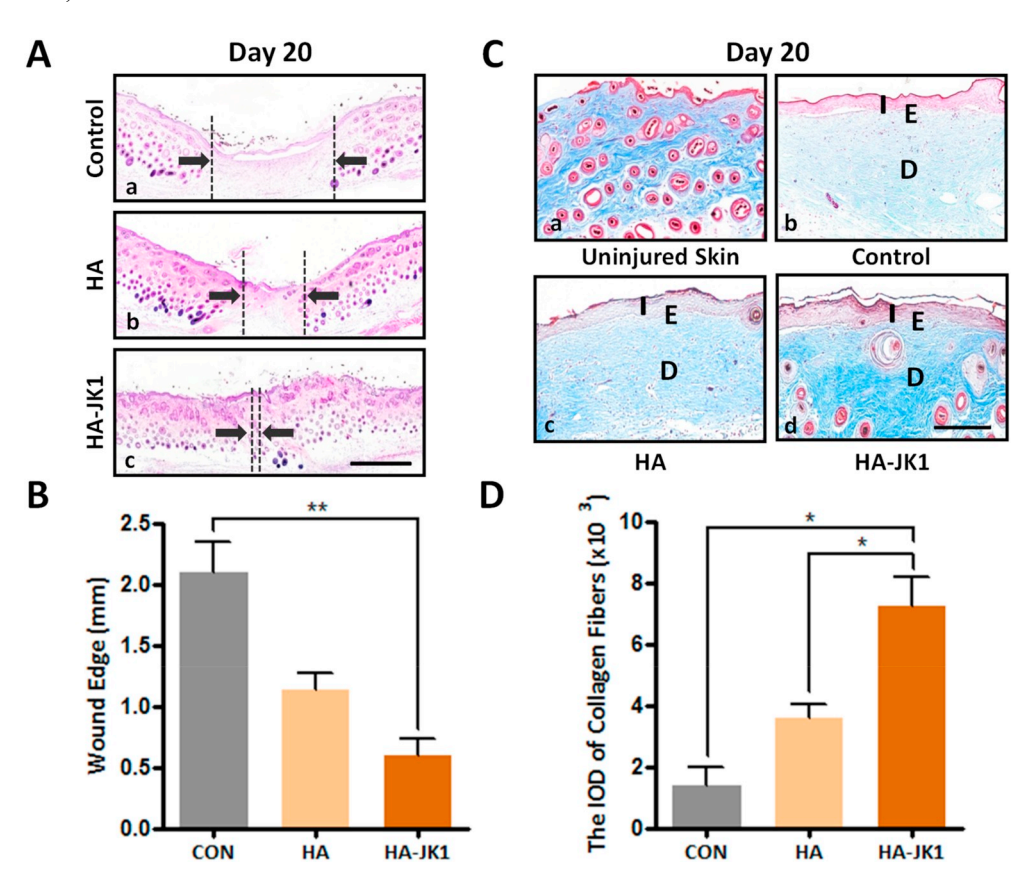


Fig. 6. Histological analysis of wound tissue sections on day 20 post treatment. (A) Representative pictures of HE staining of the control group, HA hydrogel group and HA-JK1 hydrogel group on day 20. Black arrows indicated microscopic wound edges. Scale bar: 1 mm. (B) Measurement of wound edges of the three groups on day 20, n = 3. (C) Magnified pictures of Masson's trichrome staining of the three groups on day 20. E: epidermis. D: dermis. Scale bar: 300 µm. (D) Statistical data of the collagen density of the three groups, n = 3. Statistical differences were performed using one-way analysis of variance (ANOVA). \*\*P < 0.01, \*P < 0.05.

after releasing H2S when immerged in the PBS.

#### 4.3. Releasing profile of H<sub>2</sub>S from HA-JK1 hydrogel

JK1 is a novel pH responsive donor for H<sub>2</sub>S releasing. Next H<sub>2</sub>S releasing properties of HA-JK1 hydrogel was tested in different pH conditions (pH 7.4 and 6.0). As shown in Fig. 4A-B, both JK1 and HA-JK1 hydrogel exhibited faster H<sub>2</sub>S release under pH 6.0, which triggered relatively fast release of H2S in comparison with the profile under pH 7.4 with an early burst releasing behavior. At pH 7.4 the release profile from both systems were relatively smooth with gradually releasing profile that eventually reached the plateau. However, compared with JK1 donor alone, HA-JK1 demonstrated extended H2S-relasing profiles. In particular, the peak time for H<sub>2</sub>S under pH 6.0 was about 60 min for JK1 alone, while for HA-JK1 was retard to about 180 min (Fig. 4A). The releasing half-lives of H<sub>2</sub>S was prolonged approximately 1.8 folds, compared with JK1 alone. Under pH 7.4, HA-JK1 lowered the releasing profile of H<sub>2</sub>S (Fig. 4B). And this impede releasing of H<sub>2</sub>S was not that obvious compared to pH 6.0 which was due to the original slow releasing profile of JK1 donor itself. These data suggested that HA-JK1 could significantly extend the H<sub>2</sub>S releasing time and was more suitable for clinical application. Thus, this pH-responsive property made it a desirable drug for wound healing due to the dynamic changes of pH values during the wound healing process [47]. In brief, the acidic pH value of the early healing stage that suppresses bacterial growth triggers the fast release of H<sub>2</sub>S from JK1 to immediately lower the inflammatory level of wounds in early stage. As the healing process advances, the pH value gradually increases to weak basic range which makes JK1 to temperate release H2S in a smooth manner to exert prolonged repair effects during the regenerative phase.

#### 4.4. HA-JK1 hydrogel accelerated in vivo wound healing process

Then HA-JK1 and HA hydrogel were respectively applied to the full-

thickness dermal wound model on C57BL/6 mice to observe the effect of JK1 on the healing process in vivo with saline group as control. The wounds were photographed on day 0, 7, 10, 14, 17 and 20 post wounding. From the comparison of the visual pictures of the three groups exhibited in Fig. 5A, HA-JK1 treated wounds presented accelerated wound repair process. Especially, on the last day of the observation, we could barely see the wound area of the HA-JK1 group, instead thicker hair was covered on the wound. The immunohistochemical staining of keratin of the tissue harvested on day 20 in Fig. 5A (a-c) which indicated the structure of epidermis and hair follicles in a microscopic scale gave a clearer demonstration of the wound closure underneath the covering newborn hair. In consistent with the visual healing outcome, the HA-JK1 group achieved almost complete wound regeneration with an indistinctive wound edge, thicker epidermis and better hair follicle growth in the wound center. Furthermore, wound area percentages on each time point of each group were calculated and shown in Fig. 5B. On day 10, the wound area of the control (43.8  $\pm$  9.6%) and HA group (34.6  $\pm$  16.9%) were significantly larger than HA-JK1 group (28.3 ± 8.2%). And on day 20, HA-JK1 treated wounds achieved a nearly complete heal with an average wound area of 2.71  $\pm$  3.13%. The dynamic healing process was traced in the schematic diagram in Fig. 5C to show much clearer of this healing process.

Hematoxylin-eosin (HE) staining and Masson's trichrome staining were next performed to observe granulation tissue regeneration on day 20 (Fig. 6A). The control wounds exhibited thinnest regenerative tissue in the wound center, which was thinner than the HA group, while HAJK1 applied wounds were apparently thicker and more flat. The average lengths of the wound edge indicated by black arrows were  $2.1 \pm 0.4\,\mathrm{mm}$  for the control group and  $1.1 \pm 0.2\,\mathrm{mm}$  for the HA group, which indicated slower closure rates when compared with the HA-JK1 group ( $0.6 \pm 0.2\,\mathrm{mm}$ ) (Fig. 6B). Magnified pictures of Masson's trichrome staining were shown in Fig. 6C to assess collagen deposition in terms of collagen arrangement and density of the newly

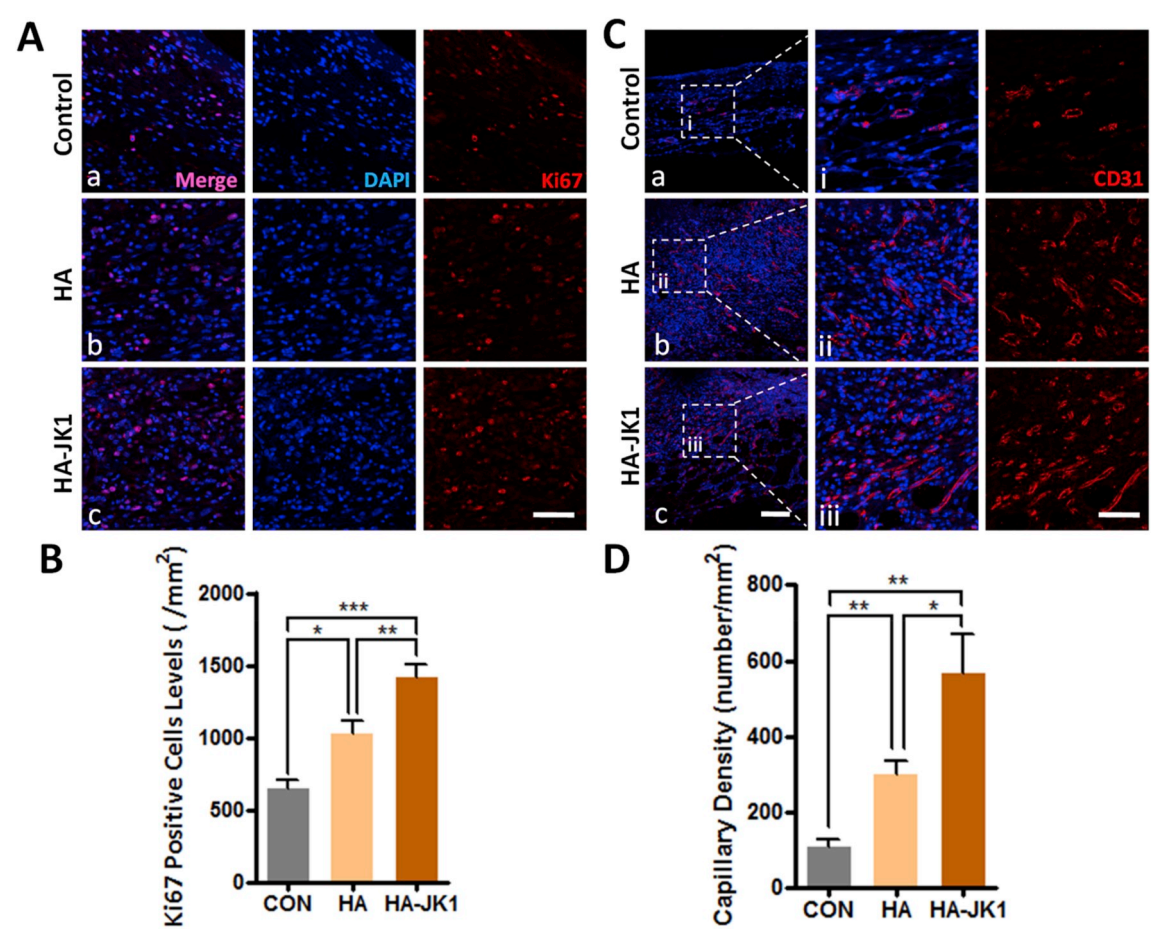


Fig. 7. HA-JK1 hydrogel enhanced cell proliferation and angiogenesis at wound site on day 7 post treatment. (A) Representative pictures of Ki67 immuno-fluorescence staining of the control group, HA hydrogel group and HA-JK1 hydrogel group on day 7. Scale bar:  $50 \,\mu\text{m}$ . (B) Statistical data of Ki67 positive cells levels of the three groups,  $n \ge 5$ . (C) Representative pictures of CD31 immunofluorescence staining of the control group, HA hydrogel group and HA-JK1 hydrogel group on day 7. Figure a–c share the scale bar of  $100 \,\mu\text{m}$ , magnified pictures of  $50 \,\mu\text{m}$ . (D) Statistical data of the capillary density of the three groups, n = 5. Statistical differences were performed using one-way analysis of variance (ANOVA). \*\*\*P < 0.001, \*\*P < 0.01, \*P < 0.05.

regenerated wound. Among all the groups, compared to the light blue collagen of control and HA hydrogel group, HA-JK1 group showed the densest and most orderly collagen bundles around with mature skin appendages close to uninjured skin. Quantitatively, according to statistics in Fig. 6D, HA-JK1 achieved an increase of collagen density [IOD:  $(7.2 \pm 1.0) \times 10^3$ ] by 2 fold and 5 fold compared with the HA [IOD:  $(3.6 \pm 0.4) \times 10^3$ ] and control group [IOD:  $(1.4 \pm 0.6) \times 10^3$ ], respectively. These results further revealed that with the addition of JK1, the main wound matrix of granulation and collagen formation were enhanced upon the wound.

In order to further confirm that the healing efficiency was accelerated by HA-JK1, we performed additional animal experiments and added free JK1 (0.04 M) and another  $\rm H_2S$  donor NaHS (0.04 M) as a positive control in the early stage of wound repair (on day 7). Wound healing efficiency as shown in Fig. S3, HA-JK1 exhibited fastest macroscopic healing rate (46.1  $\pm$  4.6% wound area) compared with free JK1 and NaHS, suggesting the potent pro-healing function of incubation of JK1 to HA hydrogel system. Except promoting M2 macrophage polarization by JK1, still JK1 needs a perfect system to help carry and sustained release versatile  $\rm H_2S$ . Free JK1 and NaHS alone without biomaterials delivery system won't help with acute wound repair, which may due to the uncontrollable or burst release of  $\rm H_2S$ . Once again, we demonstrated the significance of cooperative biomaterials with specific drug.

Further immunohistochemical staining of a H<sub>2</sub>S-generating enzymes (Cystathionine-γ-lyse, CSE) was performed to detect the specific role of

 $\rm H_2S$  as a gasotransmitter from NaHS or HA-JK1. Exogenous administration of  $\rm H_2S$  would enhance proangiogenic of wound by regulating the expressions of CSE, leading to improved wound regeneration [66]. Fig. S4 showed that compared with control and HA, there existed significant increase of CSE expressions of HA-JK1 along with NaHS, confirming the specific releasing of  $\rm H_2S$  from HA-JK1 contributing to the wound healing.

### 4.5. Cell proliferation and angiogenesis were both enhanced by HA-JK1 hydrogel

The regeneration phase is a critical step for wound healing, involving various cells participating in such as keratinocytes, fibroblasts and endothelial cells. Previous studies demonstrated that H<sub>2</sub>S had proproliferation effects on fibroblasts and vascular endothelial cells *in vitro*. [37,67] In order to investigate the effect of H<sub>2</sub>S exerting on the proliferation of cells within the wound site *in vivo*, Ki67 immunofluorescence staining was performed, which is a recognized marker of proliferating cells located in nucleus [68]. It could be visualized in Fig. 7A that on day 7, a large amount of Ki67 positive cells expressing red fluorescence existed in the dermis of the regenerating wounds. By calculating and comparing the levels of Ki67 positive cells, we found that in the control wounds, there were less cells undergoing proliferation. In contrast, the HA treatment promoted the proliferation of cells in the wounds, while significantly, the HA-JK1 group exhibited a highest density of proliferating cells (Fig. 7B), indicating the positive role of

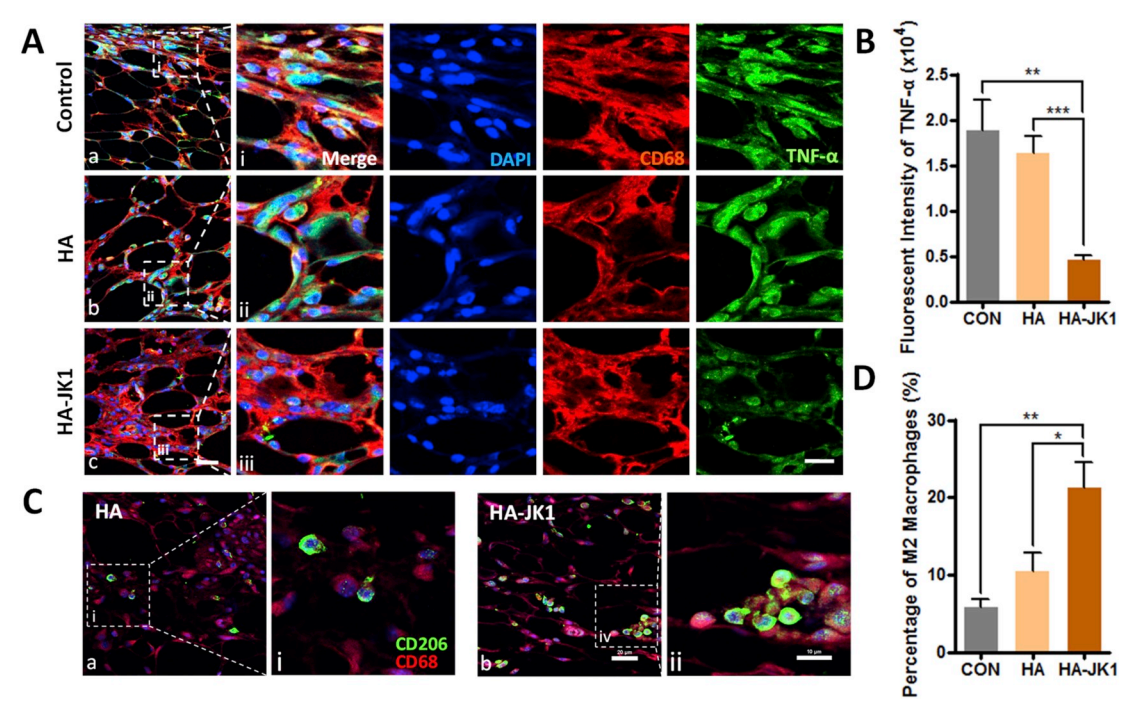


Fig. 8. HA-JK1 hydrogel alleviated inflammation level and drove more M2 macrophages polarization on day 7 post treatment. (A) Representative pictures of CD68/ TNF- $\alpha$  immunofluorescence staining of the control group, HA hydrogel group and HA-JK1 hydrogel group on day 7. Figure a–c share the scale bar of 20 μm, magnified pictures of 10 μm. (B) Statistical data of the TNF- $\alpha$  fluorescence intensity of the three groups,  $n \ge 5$ . (C) Representative pictures of CD206/CD68 immunofluorescence staining of HA hydrogel group and HA-JK1 hydrogel group on day 7 post wounding. Scale bar: 20 μm for a and b, 10 μm for i and ii. W: wound area. (D) Statistical data of the percentage of M2 macrophages of the three groups,  $n \ge 5$ . Statistical differences were performed using one-way analysis of variance (ANOVA). \*\*\*P < 0.001, \*\*P < 0.01, \*P < 0.05.

 $\rm H_2S$  released from JK1 on the proliferation of healing-associated cells, which was the very basis of the regeneration process of wound healing to promote new structure and tissue formation such as granulation tissue.

During wound healing, angiogenesis is an indispensable step with endothelial cells migrating from the unwounded sites and forming new vessels, carrying oxygen and nutrients to the wound site in support of Besides, H<sub>2</sub>S was previously reported to promote angiogenesis in vivo. [69,70] H<sub>2</sub>S also plays a part in maintaining the angiogenic function of endothelial progenitor cell (EPC) [13]. The newly formed vessels in the wounds were stained with CD31, a marker for vascular endothelial cells. The representative pictures of immunofluorescence staining in Fig. 7C and the count of capillary densities in Fig. 7D exhibited sparsely distributed vessels in the control wounds with the density of  $106.7 \pm 85.5$  capillaries/mm<sup>2</sup>. After treated with HA and HA-JK1 hydrogels, capillaries of significantly higher density were regenerated in the dermis which were 297.8 ± 48.2 capillaries/mm<sup>2</sup> and 497.8 ± 233.9 capillaries/mm<sup>2</sup>, respectively. Taken together, H<sub>2</sub>S released from HA-JK1 took additional effects on the process of cell proliferation and angiogenesis during dermal wound healing, together promoting wound closure.

## 4.6. HA-JK1 hydrogel decreased inflammation and induced in vivo macrophage polarization

Among the wound healing process, the inflammation phase initiates the whole healing process and overlaps with the subsequent regeneration phase which is of great importance to the healing outcome. To assess the inflammatory level of the wounds undergoing different treatment, TNF- $\alpha$  was chosen to be an indicator for inflammatory response and CD68 for macrophages. Macrophages expressing TNF- $\alpha$  in the subcutaneous layer of the wounds on day 7 post wounding were immunofluorescence stained and showed in Fig. 8A. The levels of TNF- $\alpha$  were relatively high in the control group [(1.9  $\pm$  0.3)  $\times$  10<sup>4</sup>] and

HA group [ $(1.6\pm0.2)\times10^4$ ] compared with the HA-JK1 applied wounds [ $(0.5\pm0.01)\times10^4$ ] which showed a significant decrease of TNF- $\alpha$  fluorescent intensity of only 24.84% and 28.44% of that of the control and HA group (Fig. 8B). In Fig. S5, immunohistochemical staining results of IL-6, another inflammation indicator, also demonstrated that HA-JK1 treatment significantly lowered the level of proinflammatory cytokines upon wound bed. These results were due to the limitation of inflammation of the HA-JK1 hydrogel by effective H<sub>2</sub>S release, which exerted prominent effects of anti-inflammation.

Since macrophages are the major type of inflammatory cells during the early healing process and their mainly two polarization directions towards M1 or M2 phenotype were intensively studied to have opposite biological effects. Besides, our in vitro study has already demonstrated that JK1 exerted obvious M2 polarization promoting effects on macrophages. Therefore, we further tested the in vivo of M2 polarization of macrophages to confirm the function of H<sub>2</sub>S released from HA-JK1. To investigate the effects of HA-JK1 to promote M2 polarization in vivo, CD206/CD68 immunofluorescence staining was performed on 7-day wound tissue sections. CD206 was chosen as an surface marker of M2 macrophages [71], and CD68 for macrophages of all the subsets. As shown in the representative fluorescent pictures in Fig. 8C, in the subcutaneous layer on the wounds, the single HA group showed fewer CD206 positive cells while the HA-JK1 group exhibited a more widely distribution of CD206 positive cells. It signified that H<sub>2</sub>S released from HA-JK1 hydrogels generated higher level of M2 macrophages in the wound sites, which was 1.9 fold more than the HA group (Fig. 8D). Moreover, M2 macrophages was necessary for cell proliferation, which could partly explain the cell proliferation promoting effects of HA-JK1 on wound healing in vivo (Fig. 7A-B). And more M2 macrophages induced by JK1 secreted more VEGFs, a major contributor to angiogenesis in wound healing [56,72], which in part contributed to the neovascularization in the wounds applied with HA-JK1 hydrogel (Fig. 7C-D). Also, we detected iNOS (a classical M1 marker) expression at wound sites on day 7 using immunohistochemical staining (Fig. S6), which

indicated a lower level of M1 macrophages in the HA-JK1 treated group compared with the control and the HA group. In summary, reparative M2 polarization induced by  $\rm H_2S$  further magnified the pro-healing function of  $\rm H_2S$  releasing HA-JK1 through playing an important role in anti-inflammation, cell proliferation and angiogenesis during the healing process.

#### 5. Conclusion

In this study, a pH controllable H<sub>2</sub>S donor JK1 was tested to show the capability to promote M2 (anti-inflammatory) phenotype of macrophages with more active pro-healing potential. The HA hydrogel could effectively encapsulate JK1, which showed pH regulated H<sub>2</sub>S releasing behavior and comparatively slower releasing rate compared to JK1 alone. The in vivo study of full-thickness removal wound healing model showed that this HA-JK1 hybrid hydrogel dressing system exhibited significant enhanced dermal regeneration efficacy compared with HA only, likely due to the cyto-protective characteristics of H2S. Finally, we found that the excellent healing effect of HA-JK1, as a novel H<sub>2</sub>S donor doped matrix, could be attributed to the enhanced cell proliferation, angiogenesis as well as macrophage polarization towards M2 phenotype in vivo. The M2 polarization of H2S toward macrophage could not only reduce inflammation response but also promote next regeneration process. We believe our HA-JK1 dressing could further be applied to delayed diabetic wound healing and other biomedical applications not only in skin tissue engineering.

#### Acknowledgement

H.H. would acknowledge the financial support from Zhejiang Provincial Natural Science Foundation of China (LGF19H180008), National Natural Science Funding of China (81701809), the Zhejiang Qianjiang Talent project (QJD1803015) and the Opening Project of Zhejiang Provincial Top Key Discipline of Pharmaceutical Sciences (YKFJ3-011). J.W. would acknowledge the financial support from National Natural Science Funding of China (81601615). Q.W. was supported in part by the NSF and SC EPSCoR/IDeA Program under NSF Award #OIA-1655740. The views, perspective, and content do not necessarily represent the official views of the SC EPSCoR/IDeA Program nor those of the NSF. We also thank, Hanzhi Ling, Xiaoying Chu from Jianguang Wang's group, Yu Wang from Xiaoxia Kong's group, and Lujia Zhou from Wenzhou medical university for their kind help in performing and analysis of flow cytometry experiment.

#### Appendix A. Supplementary data

Supplementary data to this article can be found online at https://doi.org/10.1016/j.biomaterials.2019.119398.

#### References

- [1] X. Zhao, H. Wu, B. Guo, R. Dong, Y. Qiu, P.X. Ma, Antibacterial anti-oxidant electroactive injectable hydrogel as self-healing wound dressing with hemostasis and adhesiveness for cutaneous wound healing, Biomaterials 122 (2017) 34–47.
- [2] H.S. Kim, X. Sun, J.-H. Lee, H.-W. Kim, X. Fu, K.W. Leong, Advanced drug delivery systems and artificial skin grafts for skin wound healing, Adv. Drug Deliv. Rev. (2018), https://doi.org/10.1016/j.addr.2018.12.014.
- [3] J. Wu, J. Zhu, C. He, Z. Xiao, J. Ye, Y. Li, A. Chen, H. Zhang, X. Li, L. Lin, Y. Zhao, J. Zheng, J. Xiao, Comparative study of heparin-poloxamer hydrogel modified bFGF and aFGF for in vivo wound healing efficiency, ACS Appl. Mater. Interfaces 8 (2016) 18710–18721.
- [4] J. Wu, J. Ye, J. Zhu, Z. Xiao, C. He, H. Shi, Y. Wang, C. Lin, H. Zhang, Y. Zhao, X. Fu, H. Chen, X. Li, L. Li, J. Zheng, J. Xiao, Heparin-based coacervate of FGF2 improves dermal regeneration by asserting a synergistic role with cell proliferation and endogenous facilitated VEGF for cutaneous wound healing, Biomacromolecules 17 (2016) 2168–2177.
- [5] Q. Xiang, J. Xiao, H. Zhang, X. Zhang, M. Lu, H. Zhang, Z. Su, W. Zhao, C. Lin, Y. Huang, X. Li, Preparation and characterisation of bFGF-encapsulated liposomes and evaluation of wound-healing activities in the rat, Burns 37 (2011) 886–895.
- [6] R. Geesala, N. Bar, N.R. Dhoke, P. Basak, A. Das, Porous polymer scaffold for on-site

- delivery of stem cells-protects from oxidative stress and potentiates wound tissue repair, Biomaterials 77 (2016) 1-13.
- [7] Y. Nakamura, H. Ishikawa, K. Kawai, Y. Tabata, S. Suzuki, Enhanced wound healing by topical administration of mesenchymal stem cells transfected with stromal cellderived factor-1, Biomaterials 34 (2013) 9393–9400.
- [8] P.S. Rabbani, A. Zhou, Z.M. Borab, J.A. Frezzo, N. Srivastava, H.T. More, W.J. Rifkin, J.A. David, S.J. Berens, R. Chen, S. Hameedi, M.H. Junejo, C. Kim, R.A. Sartor, C.F. Liu, P.B. Saadeh, J.K. Montclare, D.J. Ceradini, Novel lipoproteoplex delivers keap1 sirna based gene therapy to accelerate diabetic wound healing, Biomaterials 132 (2017) 1–15.
- [9] P.S. Randeria, M.A. Seeger, X.Q. Wang, H. Wilson, D. Shipp, C.A. Mirkin, A.S. Paller, Sirna-based spherical nucleic acids reverse impaired wound healing in diabetic mice by ganglioside GM3 synthase knockdown, Proc. Natl. Acad. Sci. U.S.A. 112 (2015) 5573–5578.
- [10] R. Guo, S. Xu, L. Ma, A. Huang, C. Gao, The healing of full-thickness burns treated by using plasmid DNA encoding VEGF-165 activated collagen-chitosan dermal equivalents, Biomaterials 32 (2011) 1019–1031.
- [11] T. Tokatlian, C. Cam, T. Segura, Porous hyaluronic acid hydrogels for localized nonviral DNA delivery in a diabetic wound healing model, Adv. Healthc. Mater. 4 (2015) 1084–1091.
- [12] J.D. Luo, Y.Y. Wang, W.L. Fu, J. Wu, A.F. Chen, Gene therapy of endothelial nitric oxide synthase and manganese superoxide dismutase restores delayed wound healing in type 1 diabetic mice, Circulation 110 (2004) 2484–2493.
- [13] F. Liu, D.D. Chen, X. Sun, H.H. Xie, H. Yuan, W. Jia, A.F. Chen, Hydrogen sulfide improves wound healing via restoration of endothelial progenitor cell functions and activation of angiopoietin-1 in type 2 diabetes, Diabetes 63 (2014) 1763–1778.
- [14] J. Wu, Y. Li, C. He, J. Kang, J. Ye, Z. Xiao, J. Zhu, A. Chen, S. Feng, X. Li, J. Xiao, M. Xian, Q. Wang, Novel H<sub>2</sub>S releasing nanofibrous coating for in vivo dermal wound regeneration, ACS Appl. Mater. Interfaces 8 (2016) 27474–27481.
- [15] C.C. Yates, D. Whaley, R. Babu, J. Zhang, P. Krishna, E. Beckman, A.W. Pasculle, A. Wells, The effect of multifunctional polymer-based gels on wound healing in full thickness bacteria-contaminated mouse skin wound models, Biomaterials 28 (2007) 3977–3986.
- [16] C.O. Chantre, P.H. Campbell, H.M. Golecki, A.T. Buganza, A.K. Capulli, L.F. Deravi, S. Dauth, S.P. Sheehy, J.A. Paten, K. Gledhill, Y.S. Doucet, H.E. Abaci, S. Ahn, B.D. Pope, J.W. Ruberti, S.P. Hoerstrup, A.M. Christiano, K.K. Parker, Production-scale fibronectin nanofibers promote wound closure and tissue repair in a dermal mouse model. Biomaterials 166 (2018) 96–108.
- [17] J. Xie, M.R. Macewan, W.Z. Ray, W. Liu, D.Y. Siewe, Y. Xia, Radially aligned, electrospun nanofibers as dural substitutes for wound closure and tissue regeneration applications, ACS Nano 4 (2010) 5027–5036.
- [18] J. Wu, Z. Xiao, A. Chen, H. He, C. He, X. Shuai, X. Li, S. Chen, Y. Zhang, B. Ren, J. Zheng, J. Xiao, Sulfated zwitterionic poly(sulfobetaine methacrylate) hydrogels promote complete skin regeneration, Acta Biomater. 71 (2018) 293–305.
- [19] H.L. Xu, P.P. Chen, D.L. ZhuGe, Q.Y. Zhu, B.H. Jin, B.X. Shen, J. Xiao, Y.Z. Zhao, Liposomes with silk fibroin hydrogel core to stabilize bFGF and promote the wound healing of mice with deep second-degree scald, Adv. Healthc. Mater. 6 (2017) 1700344
- [20] C. Mao, Y. Xiang, X. Liu, Z. Cui, X. Yang, K.W.K. Yeung, H. Pan, X. Wang, P.K. Chu, S. Wu, Photo-inspired antibacterial activity and wound healing acceleration by hydrogel embedded with Ag/Ag@Agcl/ZnO nanostructures, ACS Nano 11 (2017) 9010–9021.
- [21] A. Chen, H. He, G. Ma, Y. Li, S. Jiang, X. Xuan, Y. Song, C. Zhang, J. Xiao, Y. Xu, Biodegradable copolypeptide hydrogel prodrug accelerates dermal wound regeneration by enhanced angiogenesis and epithelialization, RSC Adv. 8 (2018) 10620–10626.
- [22] V. Albright, M. Xu, A. Palanisamy, J. Cheng, M. Stack, B. Zhang, A. Jayaraman, S.A. Sukhishvili, H. Wang, Micelle-coated, hierarchically structured nanofibers with dual-release capability for accelerated wound healing and infection control, Adv. Healthc. Mater. 7 (2018) 1800132.
- [23] C. Gong, Q. Wu, Y. Wang, D. Zhang, F. Luo, X. Zhao, Y. Wei, Z. Qian, A biode-gradable hydrogel system containing curcumin encapsulated in micelles for cutaneous wound healing, Biomaterials 34 (2013) 6377–6387.
- [24] J. Xiao, Y. Zhu, S. Huddleston, P. Li, B. Xiao, O.K. Farha, G.A. Ameer, Copper metalorganic framework nanoparticles stabilized with folic acid improve wound healing in diabetes, ACS Nano 12 (2018) 1023–1032.
- [25] X. Yang, J. Yang, L. Wang, B. Ran, Y. Jia, L. Zhang, G. Yang, H. Shao, X. Jiang, Pharmaceutical intermediate-modified gold nanoparticles: against multidrug-resistant bacteria and wound-healing application via an electrospun scaffold, ACS Nano 11 (2017) 5737–5745.
- [26] B. Balakrishnan, M. Mohanty, P.R. Umashankar, A. Jayakrishnan, Evaluation of an in situ forming hydrogel wound dressing based on oxidized alginate and gelatin, Biomaterials 26 (2005) 6335–6342.
- [27] K.R. Kirker, Y. Luo, J.H. Nielson, J. Shelby, G.D. Prestwich, Glycosaminoglycan hydrogel films as bio-interactive dressings for wound healing, Biomaterials 23 (2002) 3661–3671.
- [28] P. Maturavongsadit, J.A. Luckanagul, K. Metavarayuth, X. Zhao, L. Chen, Y. Lin, Q. Wang, Promotion of in vitro chondrogenesis of mesenchymal stem cells using in situ hyaluronic hydrogel functionalized with rod-like viral nanoparticles, Biomacromolecules 17 (2016) 1930–1938.
- [29] B.A. Shook, E. Xiao, Y. Kumamoto, A. Iwasaki, V. Horsley, CD301b+ macrophages are essential for effective skin wound healing, J. Investig. Dermatol. 136 (2016) 1885–1891.
- [30] M. Takeo, W. Lee, M. Ito, Wound healing and skin regeneration, Cold Spring Harbor Perspect. Med. 5 (2015) a023267.
- [31] S.A. Eming, M. Hammerschmidt, T. Krieg, A. Roers, Interrelation of immunity and

- tissue repair or regeneration, Semin, Cell Dev. Biol. 20 (2009) 517-527.
- [32] J.M. Lambert, E.F. Lopez, M.L. Lindsey, Macrophage roles following myocardial infarction, Int. J. Cardiol. 130 (2008) 147–158.
- [33] C. Wetzler, H. Kampfer, B. Stallmeyer, J. Pfeilschifter, S. Frank, Large and sustained induction of chemokines during impaired wound healing in the genetically diabetic mouse: prolonged persistence of neutrophils and macrophages during the late phase of repair, J. Investig, Dermatol. 115 (2000) 245–253.
- [34] V. Falanga, Wound healing and its impairment in the diabetic foot, Lancet 366 (2005) 1736–1743.
- [35] A. Sindrilaru, T. Peters, S. Wieschalka, C. Baican, A. Baican, H. Peter, A. Hainzl, S. Schatz, Y. Qi, A. Schlecht, J.M. Weiss, M. Wlaschek, C. Sunderkotter, K. Scharffetter-Kochanek, An unrestrained proinflammatory M1 macrophage population induced by iron impairs wound healing in humans and mice, J. Clin. Investig. 121 (2011) 985–997.
- [36] J.L. Wallace, R.W. Blackler, M.V. Chan, G.J. Da Silva, W. Elsheikh, K.L. Flannigan, I. Gamaniek, A. Manko, L. Wang, J.P. Motta, A.G. Buret, Anti-inflammatory and cytoprotective actions of hydrogen sulfide: translation to therapeutics, Antioxid. Redox Signaling 22 (2015) 398–410.
- [37] J.L. Wallace, R. Wang, Hydrogen sulfide-based therapeutics: exploiting a unique but ubiquitous gasotransmitter, Nat. Rev. Drug Discov. 14 (2015) 329–345.
- [38] A. Katsouda, S.I. Bibli, A. Pyriochou, C. Szabo, A. Papapetropoulos, Regulation and role of endogenously produced hydrogen sulfide in angiogenesis, Pharmacol. Res. 113 (2016) 175–185.
- [39] M. Gao, R. Wang, F. Yu, L. Chen, Evaluation of sulfane sulfur bioeffects via a mitochondria-targeting selenium-containing near-infrared fluorescent probe, Biomaterials 160 (2018) 1–14.
- [40] F. Yu, M. Gao, M. Li, L. Chen, A dual response near-infrared fluorescent probe for hydrogen polysulfides and superoxide anion detection in cells and in vivo, Biomaterials 63 (2015) 93–101.
- [41] N. Dufton, J. Natividad, E.F. Verdu, J.L. Wallace, Hydrogen sulfide and resolution of acute inflammation: a comparative study utilizing a novel fluorescent probe, Sci. Rep. 2 (2012) 499.
- [42] L. Miao, X. Shen, M. Whiteman, H. Xin, Y. Shen, X. Xin, P.K. Moore, Y.Z. Zhu, Hydrogen sulfide mitigates myocardial infarction via promotion of mitochondrial biogenesis-dependent M2 polarization of macrophages, Antioxid. Redox Signaling 25 (2016) 268–281.
- [43] M.D. Hartle, M.D. Pluth, A practical guide to working with H<sub>2</sub>S at the interface of chemistry and biology, Chem. Soc. Rev. 45 (2016) 6108–6117.
- [44] Y. Zhao, S.G. Bolton, M.D. Pluth, Light-activated COS/H<sub>2</sub>S donation from photocaged thiocarbamates, Org. Lett. 19 (2017) 2278–2281.
- [45] C.T. Yang, Z.Z. Lai, Z.H. Zheng, J.M. Kang, M. Xian, R.Y. Wang, K. Shi, F.H. Meng, X. Li, L. Chen, H. Zhang, A novel pH-controlled hydrogen sulfide donor protects gastric mucosa from aspirin-induced injury, J. Cell. Mol. Med. 21 (2017) 2441–2451.
- [46] J. Kang, Z. Li, C.L. Organ, C.M. Park, C.T. Yang, A. Pacheco, D. Wang, D.J. Lefer, M. Xian, pH-controlled hydrogen sulfide release for myocardial ischemia-reperfusion injury, J. Am. Chem. Soc. 138 (2016) 6336–6339.
- [47] L.A. Schneider, A. Korber, S. Grabbe, J. Dissemond, Influence of pH on wound-healing: a new perspective for wound-therapy? Arch. Dermatol. Res. 298 (2007) 413–420.
- [48] R.A. Peattie, A.P. Nayate, M.A. Firpo, J. Shelby, R.J. Fisher, G.D. Prestwich, Stimulation of in vivo angiogenesis by cytokine-loaded hyaluronic acid hydrogel implants. Biomaterials 25 (2004) 2789–2798.
- [49] S. Gerecht, J.A. Burdick, L.S. Ferreira, S.A. Townsend, R. Langer, G. Vunjak-Novakovic, Hyaluronic acid hydrogel for controlled self-renewal and differentiation of human embryonic stem cells, Proc. Natl. Acad. Sci. U.S.A. 104 (2007) 11298–11303.
- [50] A.T. Wu, T. Aoki, M. Sakoda, S. Ohta, S. Ichimura, T. Ito, T. Ushida, K.S. Furukawa, Enhancing osteogenic differentiation of MC3T3-E1 cells by immobilizing inorganic polyphosphate onto hyaluronic acid hydrogel, Biomacromolecules 16 (2015)

- 166-173.
- [51] S. Baranoski, Wound dressings: challenging decisions, Home Healthc. Nurse 17 (1999) 19–25.
- [52] R.A. Marklein, J.A. Burdick, Controlling stem cell fate with material design, Adv. Mater. 22 (2010) 175–189.
- [53] K.A. Smeds, A. Pfister-Serres, D. Miki, K. Dastgheib, M. Inoue, D.L. Hatchell, M.W. Grinstaff, Photocrosslinkable polysaccharides for in situ hydrogel formation, J. Biomed. Mater. Res. 54 (2001) 115–121.
- [54] F.O. Martinez, L. Helming, S. Gordon, Alternative activation of macrophages: an immunologic functional perspective, Annu. Rev. Immunol. 27 (2009) 451–483.
- [55] X. Zhang, D.M. Mosser, Macrophage activation by endogenous danger signals, J. Pathol. 214 (2008) 161–178.
- [56] C.J. Ferrante, S.J. Leibovich, Regulation of macrophage polarization and wound healing, Adv. Wound Care 1 (2012) 10–16.
- [57] Y. Jia, W. Yang, K. Zhang, S. Qiu, J. Xu, C. Wang, Y. Chai, Nanofiber arrangement regulates peripheral nerve regeneration through differential modulation of macrophage phenotypes, Acta Biomater. 83 (2019) 291–301.
- [58] T.U. Luu, S.C. Gott, B.W. Woo, M.P. Rao, W.F. Liu, Micro- and nanopatterned topographical cues for regulating macrophage cell shape and phenotype, ACS Appl. Mater. Interfaces 7 (2015) 28665–28672.
- [59] S. Gao, Y. Wang, D. Li, Y. Guo, M. Zhu, S. Xu, J. Mao, G. Fan, Tanshinoneiia alleviates inflammatory response and directs macrophage polarization in lipopoly-saccharide-stimulated Raw 264.7 cells, Inflammation 42 (2018) 264–275.
- [60] F.Y. McWhorter, C.T. Davis, W.F. Liu, Physical and mechanical regulation of macrophage phenotype and function, Cell. Mol. Life Sci. 72 (2015) 1303–1316.
- [61] F.Y. McWhorter, T. Wang, P. Nguyen, T. Chung, W.F. Liu, Modulation of macrophage phenotype by cell shape, Proc. Natl. Acad. Sci. U.S.A. 110 (2013) 17253–17258.
- [62] I.S. Kim, H.C. Park, H. Quan, Y. Kim, L. Wu, H.C. Yang, Effects of triethylene glycol dimethacrylate and hydroxyethyl methacrylate on macrophage polarization, Int. Endod. J. 52 (2019) 987–998.
- [63] M. Waters, P. VandeVord, M. Van Dyke, Keratin biomaterials augment anti-inflammatory macrophage phenotype in vitro, Acta Biomater. 66 (2018) 213–223.
- [64] D.Y. Vogel, E.J. Vereyken, J.E. Glim, P.D. Heijnen, M. Moeton, P. van der Valk, S. Amor, C.E. Teunissen, J. van Horssen, C.D. Dijkstra, Macrophages in inflammatory multiple sclerosis lesions have an intermediate activation status, J. Neuroinflammation 10 (2013), https://doi.org/10.1186/1742-2094-10-35.
- [65] F. Porcheray, S. Viaud, A.C. Rimaniol, C. Leone, B. Samah, N. Dereuddre-Bosquet, D. Dormont, G. Gras, Macrophage activation switching: an asset for the resolution of inflammation, Clin. Exp. Immunol. 142 (2005) 481–489.
- [66] F. Liu, D.-D. Chen, X. Sun, H.-H. Xie, H. Yuan, W. Jia, A.F. Chen, Hydrogen sulfide improves wound healing via restoration of endothelial progenitor cell functions and activation of angiopoietin-1 in type 2 diabetes, Diabetes 63 (2014) 1763–1778.
- [67] S. Feng, Y. Zhao, M. Xian, Q. Wang, Biological thiols-triggered hydrogen sulfide releasing microfibers for tissue engineering applications, Acta Biomater. 27 (2015) 205–213
- [68] T. Scholzen, J. Gerdes, The Ki-67 protein: from the known and the unknown, J. Cell. Physiol. 182 (2000) 311–322.
- [69] A. Papapetropoulos, A. Pyriochou, Z. Altaany, G. Yang, A. Marazioti, Z. Zhou, M.G. Jeschke, L.K. Branski, D.N. Herndon, R. Wang, C. Szabo, Hydrogen sulfide is an endogenous stimulator of angiogenesis, Proc. Natl. Acad. Sci. U.S.A. 106 (2009) 21972–21977.
- [70] M.J. Wang, W.J. Cai, N. Li, Y.J. Ding, Y. Chen, Y.C. Zhu, The hydrogen sulfide donor NaHS promotes angiogenesis in a rat model of hind limb ischemia, Antioxid, Redox Signaling 12 (2010) 1065–1077.
- [71] A.C. Labonte, A.C. Tosello-Trampont, Y.S. Hahn, The role of macrophage polarization in infectious and inflammatory diseases, Mol. Cells. 37 (2014) 275–285.
- [72] N.N. Nissen, P.J. Polverini, A.E. Koch, M.V. Volin, R.L. Gamelli, L.A. DiPietro, Vascular endothelial growth factor mediates angiogenic activity during the proliferative phase of wound healing, Am. J. Pathol. 152 (1998) 1445–1452.